









Neutralization of low-energy Ne⁺ colliding with MoS₂ and metallic molybdenum: An experimental and theoretical study

P. F. Buitrago ¹, M. A. Romero ^{1,2}, C. J. Bonin ^{1,2}, Y. Irusta ^{3,4}, C. González ^{3,4}, R. Vidal ^{1,2},
Evelina A. García ¹ and F. Bonetto ^{1,2,*}

¹*Instituto de Física del Litoral (UNL-CONICET), Güemes 3450, Santa Fe, Argentina*

²*Departamento de Física, Facultad de Ingeniería Química, Santiago del Estero 2829, Santa Fe, Argentina*

³*Departamento de Física de Materiales, Universidad Complutense de Madrid, 28040 Madrid, Spain*

⁴*Instituto de Magnetismo Aplicado (UCM-ADIF), Vía de Servicio A-6, 900, 28232 Las Rozas de Madrid, Spain*



(Received 5 April 2024; accepted 18 June 2024; published 11 July 2024)

The neutralization probability in the scattering of Ne⁺ ions by a molybdenum disulfide semiconductor (MoS₂) surface in a backscattering geometric configuration is experimentally and theoretically analyzed. The low-energy ion scattering technique was used to experimentally determine the neutral fractions of Ne projectiles backscattered by the Mo atoms of the MoS₂ target surface after a single collision. A high neutralization rate in the backscattered projectiles (of the order of 95%) was obtained, practically independent of the projectile incoming energy and the collision geometry. Additionally, the remaining dispersed ions were measured to be all positive, within the experimental error. An identical experiment was conducted on a polycrystalline metallic molybdenum surface to assess for differences between the two target surfaces, with completely different electronic properties. A quantum-mechanical formalism was employed to theoretically describe the projectile-surface resonant charge transfer during the binary collision of Ne projectiles with both surfaces. Our calculations show that the inner states of Mo atoms play a central role in the resonant charge transfer in the Ne/MoS₂ system. From the comparison with the experimental results, we can conclude that the resonant charge transfer to the projectile ground state is not sufficient to explain the large neutralization of the Ne projectiles observed for both surfaces. An Auger neutralization mechanism and resonant charge transfer to the excited states of the projectile are expected to be particularly relevant for polycrystalline Mo and MoS₂ target surfaces, respectively.

DOI: [10.1103/PhysRevA.110.012806](https://doi.org/10.1103/PhysRevA.110.012806)

I. INTRODUCTION

Two-dimensional structured materials play a key role in the current development of nanoscience and nanotechnology. In addition to the well-known carbon based two-dimensional (2D) materials, transition metal chalcogenides (TMDs) and metal oxide layers present unique electrical properties that make them suitable for the next generation of superconductors, metallic/semimetallic materials, semiconductors, and insulators [1]. TMDs, like molybdenum sulfides, emerge as promising candidates for potentially replacing platinum electrodes in acidic solutions or for electrolytic production of hydrogen in fuel cells due to their stability, affordability, nontoxicity, and natural abundance [2]. Particularly in monolayer molybdenum disulfide (MoS₂), effects from dimensional reduction such as quantum confinement and intense photoluminescence, enable the construction of interband field-effect transistors promising lower power consumption than classical transistors [3].

The charge exchange between projectile atoms and surfaces during dynamic interactions involves complex interconnected mechanisms that are not yet completely understood [4–7]. Depending on the specific projectile/surface system

under investigation, this phenomenon usually exhibits a pronounced dependence on two experimentally adjustable parameters: the projectile incoming energy and the collisional geometry (scattering, incoming and exit angles; and crystallographic direction explored through the independently controlled azimuthal angle of the sample). While the former is directly associated with the projectile-surface interaction time, the second parameter predominantly determines which specific atoms on the surface will effectively interact with the projectile. The characteristic timescale of the charge exchange processes is generally in the picosecond range, leading to collisional experiments in the low- to very low-energy regime (0.5–10 keV) [8–10].

For approximately four decades, the low-energy ion scattering (LEIS) technique [11–15] has served as a valuable tool for investigating charge transfer in dynamic interactions between projectiles and surfaces. Owing to its notable surface sensitivity, LEIS has found widespread application in the study of charge transfer across various projectile-target systems [16–36]. Noble inert gases have been prevalent as projectiles in a substantial number of these studies [17,18,21,22,28,31,34–36]. However, when employing heavy ions as projectiles, it becomes imperative to utilize sufficiently low irradiation doses and incoming energies to prevent significant surface damage within the experimental time frame [37]. Notably, investigations have revealed a high neutralization

*Contact author: bonetto@santafe-conicet.gov.ar

rate when helium (He), neon (Ne), or argon (Ar) projectiles impinge upon a diverse range of metals [18,21,22,31,34] and two-dimensional structured materials such as graphite [28,35,36].

The present work is aimed to experimentally and theoretically analyze the charge exchange of Ne^+ projectiles after being backscattered by a MoS_2 surface in the low-energy regime (2–8 keV). When a Ne^+ projectile is scattered by a MoS_2 surface, binary collisions with S or Mo atoms take place. Due to the extremely low cross section of Ne-S collisions for large scattering angles in the low-energy regime, the corresponding binary collision peak can be barely detected by LEIS in reasonable experimental times. On the contrary, the Ne-Mo binary peak can be straightforwardly detected, so the present work is focused on the charge exchange of Ne projectiles singly colliding with Mo atoms of the MoS_2 surface. For comparison, we also studied the charge exchange of Ne projectiles that binary collide with Mo atoms of a polycrystalline metallic surface. The experimental study explores a large range of projectiles incoming energies (2–8 keV), two incoming/exit angle combinations, and two distinct crystallographic directions.

From the theoretical side, we employed a formalism based on the Anderson model [38] under the *spinless* approximation [39] to describe the resonant charge transfer during the Ne-Mo low-energy collisions. Resonant mechanisms, when present, are dominant over other neutralization channels such as Auger processes [40]. Our model incorporates specific details such as the influence of the neighboring S or Mo atoms and the electronic band structure of the surface along the trajectory of the projectile. Given the distinctive features of noble gases, where the relevant electronic energy level is positioned deeply relative to the surface Fermi level, we only consider two charge states simultaneously for the projectile: neutral or positively charged. The theoretical model developed in our group, with the different approximations regarding electronic correlation, has succeeded in describing the charge exchange process in numerous projectile/surface systems [26,33,36,41–47]. Several of these studies include noble gases as projectiles and 2D structured materials or thin films as targets [25,33,35,36,42,44].

Experimentally, we found that Ne^+ projectiles are almost completely neutralized when they are backscattered by Mo atoms of a MoS_2 surface. Residual non-neutralized Ne projectiles remain positively charged. Notably, this result is independent of the projectile incoming energy, the geometric configuration of the collision, or the crystallographic direction investigated. Similar trends were identified in the case of the metallic Mo sample, albeit with a decreasing neutralization rate as the incoming projectile energy increases.

The theoretical findings and their comparison with experimental results lead us to conclude on the relevance of resonant charge transfer mechanisms in both studied surfaces. Furthermore, our observations indicate that Auger neutralization mechanisms govern charge exchange in collisions of Ne with metallic Mo, and that Ne projectile excited states might play a crucial role in the charge exchange of Ne backscattered by a MoS_2 surface.

II. EXPERIMENT

We use the LEIS technique [8,14,15] to measure the final charge state of positively charged neon ions (Ne^+) after they are scattered by a $2H$ phase molybdenum disulfide ($2H\text{-MoS}_2$) surface. In short, the device available in our laboratory consists of an ion source where the ions are produced and accelerated, a Wien filter that allows for projectiles charge/mass ratio differentiation, and a time-of-flight (TOF) detector [48]. The system is located inside an ultrahigh-vacuum (UHV) chamber with a base pressure of 10^{-9} mbar. The low-energy electron diffraction (LEED) and Auger spectroscopy techniques are also available within the same chamber for crystallographic, elemental, and chemical characterization of the sample.

The Ne^+ ions are produced in the interior of a Colutron ion source and subsequently accelerated and mass filtered by a velocity filter. After that, the ion beam is pulsed and focused before impacting the $2H\text{-MoS}_2(0001)$ monocrystalline target. The impinging beam should be pulsed in order to avoid significant target damage during the experiment. The scattered projectiles are detected at the end of the 157-cm flight tube, positioned at an angle of 135° relative to the incident direction (scattering angle). The angular acceptance of the detector is 0.4° , ensuring precise filtering of the projectiles that are scattered at 135° from the incident direction. Consequently, this results in a low spread (around 0.04%) in the distances of closest approach for the detected single-scattered projectiles.

The MoS_2 target is mounted on a sample holder where the incoming (α) and exit (β) angles can be continuously varied. For the present experiment, we used $\alpha/\beta = 45^\circ/90^\circ$, where both angles are measured with respect to the surface plane [see Fig. 1(a)]. This geometrical configuration choice is based on the consideration that the exit angle β matches the exit angle of the collisional geometry used in the theoretical model: $\alpha/\beta = 90^\circ/90^\circ$ [see Fig. 1(b)]. The dependence of the charge transfer with the azimuthal angle was also experimentally evaluated for two crystallographic different azimuthal directions. The two nonequivalent crystallographic orientations were assessed by LEED [inset of Fig. 1(a)] [49,50].

The MoS_2 crystal was mechanically exfoliated in air with adhesive tape. In order to remove a large area layer, the tape was stuck close to one edge of the sample (without rubbing it) and then lifted. Immediately after exfoliation, the sample was introduced into the UHV chamber to minimize surface contamination. Once inside the chamber, the MoS_2 crystal was heated to ~ 600 K for 60 min. Subsequently, the sample was checked by Auger electron spectroscopy to be free of contaminants (C or O). For Mo polycrystalline, the sample was cleaned by Ar^+ sputtering (dc current of 400 nA) during approximately 3 h prior to each set of measurements. The efficiency of the cleaning process was confirmed through forward-scattering LEIS spectra, capable of detecting the presence of potential contaminants like carbon or oxygen.

The time-of-flight distributions of the detected particles are obtained as explained in previous works [9,33,44,51,52]. Briefly, the same voltage pulse used for pulsating the incident beam is used as a triggering starting pulse in a microchannel scaler (MCS; Ortec). A scheme of the general experimental setup can be observed in Fig. 2(a). The detected particles

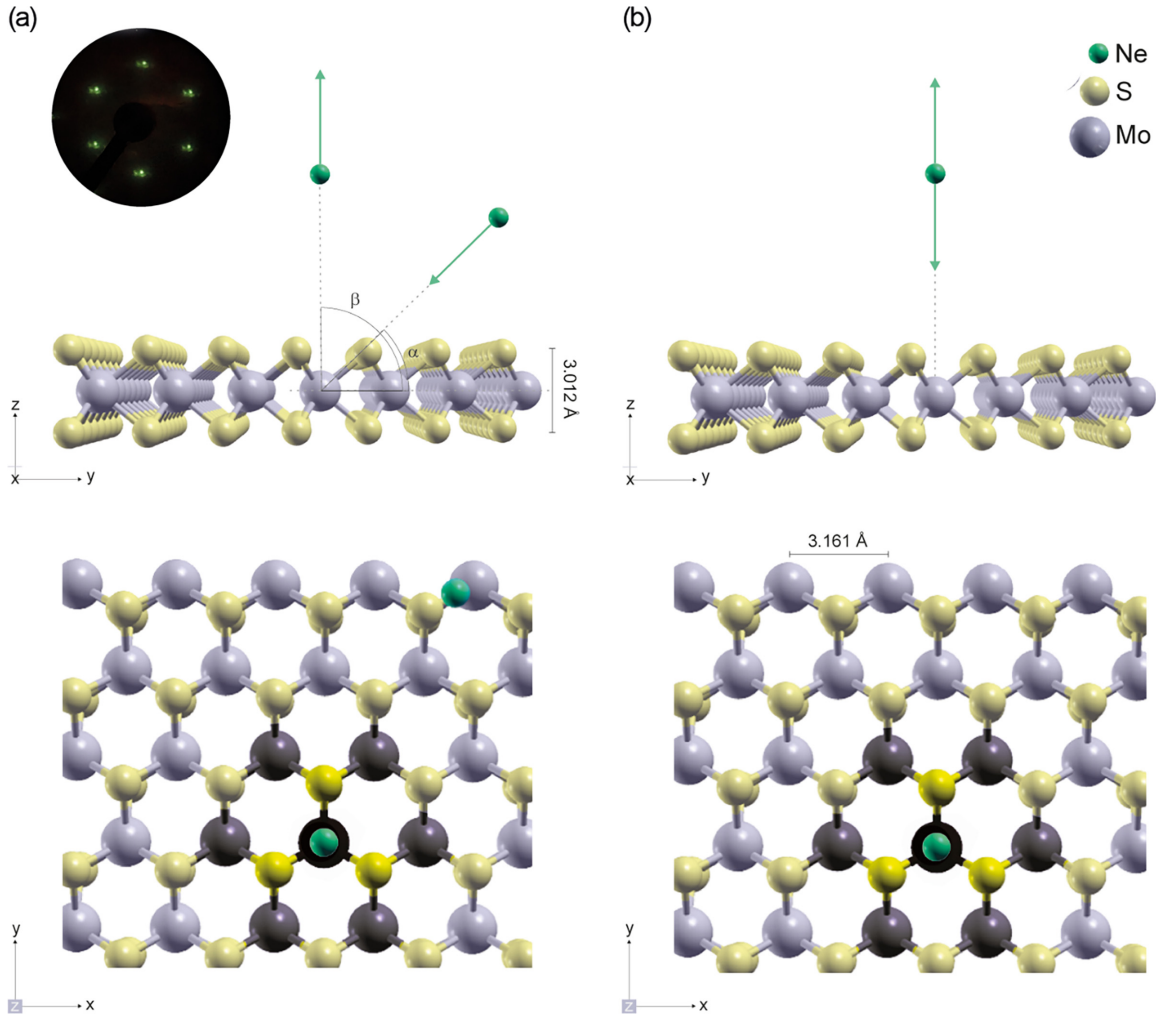


FIG. 1. Experimental (a) and theoretical (b) geometrical configuration of the collisional system studied. Lateral and top views can be seen in the upper and lower panels, respectively. In the top view the S and Mo nearest neighbors to the Mo scatter atom are highlighted in darker colors. Panel (a) corresponds to one of the azimuthal configurations experimentally studied. The corresponding LEED pattern for an electron energy of 100 eV is shown in the inset. The relevant Mo-Mo atomic distance, the layer thickness, and the incoming/exit angles are also indicated.

generate a voltage pulse at a particular time channel of the MCS and, therefore, a histogram of the number of counts detected (proportional to the number of particles reaching the detector) vs TOF (TOF spectrum) can be obtained [Fig. 2(b)]. Depending on the signal intensity, the time resolution (channel width) can be varied within certain margins, ranging from 40 to 200 ns in the present work. The minimum time resolution allowed by our spectrometer is 5 ns.

For experimentally obtaining the percentage of neutral scattered particles, total (ions plus neutrals) and only neutral scattered Ne projectiles are separated by a first pair of deflecting plates located at the entrance of the drift tube [Fig. 2(a)]. Later, they are collected by the same microchannel plates at the end of the drift tube in two independent experiments. For each incident energy, the experiment is repeated approximately ten times to gather sufficient statistical data while monitoring and keeping a constant incident current on the sample. Given that we want to describe the charge exchange processes occurring in Ne-Mo binary collisions, the neutral fraction is obtained via integrating a small TOF

window around the elastic peak position [shaded region in Fig. 2(b), around 200 ns] [9]. The final neutral fraction F is calculated as $F = N/T$, where N and T are the corresponding background-subtracted TOF spectra intensities (number of counts in the integrated region) of neutral and total scattered particles, respectively. A similar procedure was employed for determining the positive and negative scattered ion fractions [42], via applying a precalibrated voltage to a second set of deflecting plates located in front of the detector [see inset of Fig 2(a)].

III. THEORETICAL CALCULATIONS: RESONANT NEUTRAL FRACTION

A. General aspects

The model here presented attempts to properly describe the dynamic interactions between a surface of MoS₂(0001) with a Ne atom. Additionally, and for comparison, the dispersion of Ne on a polycrystalline Mo surface is also examined. The description of this scattering process is suitably provided by

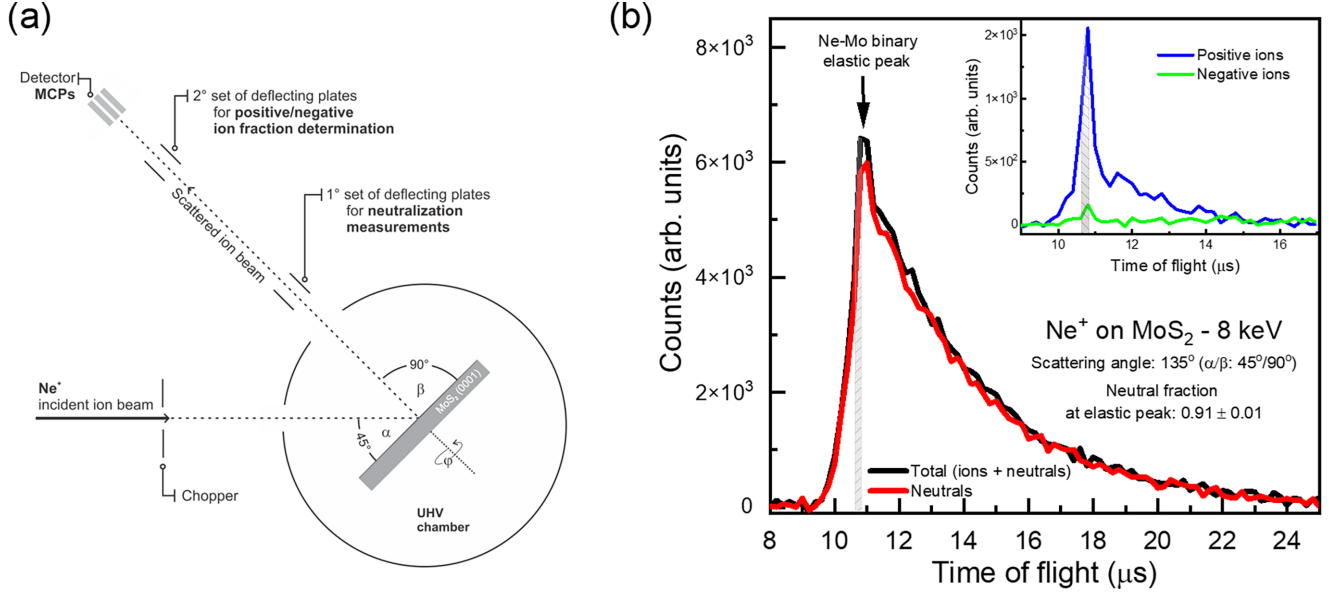


FIG. 2. (a) Scheme of the employed experimental setup. The incident (α), exit (β), scattering ($\alpha + \beta$), and azimuthal (φ) angles are indicated. Two different pairs of α/β were used in this study: $\alpha/\beta = 45^\circ/90^\circ$ and $90^\circ/45^\circ$. (b) Background-subtracted LEIS-TOF spectra obtained for total and neutral particles for 8 keV incident Ne^+ ions. The shadowed region (around 200 ns) corresponds to the theoretical Ne-Mo binary collision and it is used for obtaining the final scattered neutral fractions. The corresponding TOF spectra for positive and negative ions are shown in the inset. Predominantly positive ions are scattered from the surface.

the Anderson model [53], which furnishes the Hamiltonian for this analysis:

$$\hat{H} = \hat{H}_{\text{proj}} + \hat{H}_{\text{surf}} + \hat{H}_{\text{proj-surf}}. \quad (1)$$

The first term on the right side of Eq. (1) purely describes the Ne projectile electronic levels; the second term portrays the electronic structure of the solid MoS_2 (or Mo polycrystalline) surface, and the last term represents the interaction between the target surface and the projectile atom during the scattering process.

When feasible, resonant charge exchange mechanisms tend to be dominant [41,54]. Therefore, and in case the projectile ground state can resonate with the surface valence band, a resonant neutralization to the ground state of Ne should be expected. This neutralization process is associated to the charge fluctuation $\text{Ne}^+(1s^2 2s^2 2p^5) \leftrightarrow \text{Ne}^0(1s^2 2s^2 2p^6)$. The most complete calculation consistent with the Hamiltonian of Eq. (1) corresponds to a correlated treatment of the projectile atomic configurations. However, under certain conditions, it is convenient to perform approximations to make the calculations simpler. In this work, and as the projectile is a noble gas with filled shells, we applied the *spinless* approximation, where atomic orbitals are treated independently and the spin of the relevant electron is disregarded [32,55–57]. Even when the spinless approximation is the simplest among the three approaches regularly used within our theoretical model, it has been demonstrated to be adequate for describing the charge transfer processes when noble gases act as projectiles [35,36,56,58]. Thus, in the spinless Anderson Hamiltonian there will be only one active electronic energy level that admits one electron:

$$\hat{H} = E_a(t)\hat{n}_a(t) + \sum_{\vec{k}} \varepsilon_{\vec{k}} \hat{n}_{\vec{k}} + \sum_{\vec{k}} [V_{\vec{k}a} \hat{c}_{\vec{k}}^\dagger \hat{c}_a + \text{c.c.}], \quad (2)$$

where E_a corresponds to the energy of the active state of the atom projectile (ionization level in our particular problem) and \vec{k} denotes the surface states with energy $\varepsilon_{\vec{k}}$ and $\hat{n}_{\vec{k}} = \hat{c}_{\vec{k}}^\dagger \hat{c}_{\vec{k}}$ its occupation number. The hopping integral $V_{\vec{k}a}$ represents the coupling between the \vec{k} -surface state and the active a orbital of the projectile atom. In the problem presented here, the parameters E_a and $V_{\vec{k}a}$ are time dependent since the projectile position relative to the target surface changes with time along the collision process.

The hopping parameters $V_{\vec{k}a}$ are calculated using to the bond pair model [38]. Then, $V_{\vec{k}a}(\vec{R}(t))$ is finally expressed as a superposition of the dimeric atomic hopping integrals $V_{i\vec{R}_S,a}$ between the atomic states $\phi_{i\vec{R}_S}$ of an atom at position \vec{R}_S of the surface, and the projectile atomic state, ϕ_a , at position $\vec{R}(t)$ relative to the origin of an arbitrary coordinates system (usually chosen at the surface scatter atom). Then, the final expression for the hopping terms is

$$V_{\vec{k}a}(\vec{R}(t)) = \sum_{i\vec{R}_S} c_{i\vec{R}_S}^{\vec{k}} V_{i\vec{R}_S,a}(\vec{R}(t) - \vec{R}_S(t)). \quad (3)$$

In Eq. (3) the parameters $c_{i\vec{R}_S}^{\vec{k}}$ are the expansion coefficients of the solid surface wave function expressed as a linear combination atomic orbital (LCAO) of the target-surface \vec{k} states centered at the position \vec{R}_S of the surface atoms. They are related to the density matrix elements of the solid $\rho_{i\vec{R}_S,j\vec{R}_{S'}}(\varepsilon)$ through

$$\rho_{i\vec{R}_S,j\vec{R}_{S'}}(\varepsilon) = \sum_{\vec{k}} c_{i\vec{R}_S}^{\vec{k}*} c_{j\vec{R}_{S'}}^{\vec{k}} \delta(\varepsilon - \varepsilon_{\vec{k}}). \quad (4)$$

The atomic states of the Ne projectile atom and the S and Mo surface atoms are described by using the most accurate Huzinaga Gaussian basis sets [59,60].

B. Description of the dynamical collision process

The time dependence of the scattering process originates in the motion of the projectile relative to the target surface. For a projectile with a linear trajectory, with incoming/exit velocities $\vec{v}_{\text{in/out}}$ relative to a coordinate system with origin in the scatter atom, the position vector $\vec{R}(t)$ is

$$\vec{R}(t) = \vec{R}(0) + \vec{v}_{\text{in/out}}t, \quad (5)$$

where $\vec{R}(0)$ corresponds to the point where the distance of closest approach is reached or the return point (rtp). For the present collisional system, Ne on Mo with a scattering angle of 135° , the distance of closest approach ranges from approximately 1 a.u. (atomic units) at 2 keV to 0.5 a.u. at 8 keV, based on calculations using the Ziegler, Biersack, and Littmark or Thomas-Fermi-Moliere interaction potentials [61]. However, due to our calculations becoming unstable for ion-surface distances below 1 a.u., we decided to fix this distance at 1 a.u. Despite this limitation, the approximation can be justified since we found only a very slight dependence of the calculated neutral fraction with the distance of closest approach within a relevant range of projectile-surface distances (between 1 and 2 a.u.).

Trajectories normal to the surface ($\vec{R}(t) = z(t)\hat{k}$) and constant velocities (\vec{v}_{in} and \vec{v}_{out}) are assumed for the incoming and exit paths, respectively. The exit kinetic energy of the projectile is calculated as $E_{\text{out}} = \lambda E_{\text{in}}$, being λ the kinematic loss factor for the experimental scattering angle (135°). Then, $\lambda = 0.48$ for the Ne-Mo binary collision [8].

To theoretically determine the charge state of Ne projectiles at the time t during its interaction with the surface, we use the nonequilibrium Green-Keldysh functions formalism [62]. Under the spinless approximation, these functions reduced to

$$\begin{aligned} G_{aa}(t, t') &= i\theta(t' - t)\langle\{\hat{c}_a^\dagger(t'), \hat{c}_a(t)\}\rangle, \\ F_{aa}(t, t') &= i\langle[\hat{c}_a^\dagger(t'), \hat{c}_a(t)]\rangle, \end{aligned} \quad (6)$$

where $[,]$ and $\{,\}$ indicate commutator and anticommutator, respectively. The Green's functions are solved by using an equations of motion method [39]. The neutralization probability is then given by the average occupation of the relevant atomic state $\langle\hat{n}_a(t)\rangle$ [58], and it is obtained from the Keldysh function $F_a(t, t')$ at equal times $t = t'$:

$$\langle\hat{n}_a(t)\rangle = \frac{1}{2}[1 - iF_{aa}(t, t)]. \quad (7)$$

The neutralization (P^0) and ionization (P^+) probabilities at time t are calculated as

$$\begin{aligned} P^0(t) &= \langle\hat{n}_a(t)\rangle, \\ P^+(t) &= 1 - \langle\hat{n}_a(t)\rangle. \end{aligned} \quad (8)$$

C. Density matrix of MoS₂ and polycrystalline Mo

To derive the neutralization probability described in Eq. (8), it is essential to provide a precise description of the target surface via the coefficients $c_{j\vec{R}_S}^k$ [Eq. (4)]. Thus, and even when the projectile ion directly interacts with a limited number of surface atoms, the extended nature of the target surface comes into play through the density matrix coefficients $\rho_{i, \vec{R}_S j, \vec{R}_S}$.

The density matrix coefficients of the two target surfaces studied (MoS₂ and Mo) were calculated using the density functional theory (DFT) implemented in the FIREBALL package [63], where the LCAOs approximation was used to describe the wave function of the solid targets. This code uses the multicenter weighted exchange-correlation density approximation [64] expression for the local density approximation for the exchange and correlation functional as well as the Troullier-Martins pseudopotentials [65]. The mentioned orbitals vanish for a certain cutoff radius, drastically reducing the number of interactions and speeding up the calculations. In our simulations, the following cutoff radii, r_c , have been used for each orbital: $r_c(s) = 3.9(5.0)$ a.u., $r_c(p) = 4.5(4.5)$ a.u., and $r_c(d) = 5.0(4.8)$ a.u. for sulfur (molybdenum), respectively. The basis has been successfully tested in previous studies [66], obtaining a good agreement with both the atomic and the electronic structure. For the MoS₂ surface, we found a lattice parameter of 3.20 Å close to the experimental value (3.15 Å) [67] and the change from the direct to the indirect gap has been observed as the number of layers in the system increases from a unique monolayer to the bulk. In a first step, the MoS₂ surface has been relaxed using a 5×5 superficial unit cell including four layers with its corresponding bulk stacking (300 atoms) [67]. In a second step, the Mo surface has been created with eight layers in the slab, and a 5×5 periodicity (400 atoms) in the unit cell. Both materials have been sampled with 16 k points in the first Brillouin zone. For both systems, the density matrix has been calculated taking the Hamiltonian (H) from the DFT relaxation and using the standard equation given by

$$\rho_{mn}(\varepsilon) = \frac{1}{\pi} \text{Im}[I(\varepsilon \pm i\eta) - H]_{mn}^{-1}, \quad (9)$$

where m and n summarizes atom and state indices $[i, \vec{R}_S$ and j, \vec{R}_S , respectively as in Eq. (4)], ε is the energy, I is the identity matrix, and η is a small value that gives a broadening to the atomic states avoiding mathematical problems with the zeros in the denominator.

For the present study and in order to ensure proper convergence of the ionization level and its hybridization functions [68], it is necessary to include 10 atoms in our scattering model (Mo scatter plus three neighboring S atoms and six Mo atoms) in the case of a MoS₂ surface (shown as highlighted atoms in darker colors in the lower panels of Fig. 1); and 11 atoms (Mo scatter plus 10 neighboring Mo atoms) in the case of the metallic Mo polycrystalline.

IV. RESULTS AND DISCUSSION

A. Experimental results: Measured neutral fractions

Figure 3(a) shows the neutral fractions measured by LEIS for the binary collision of Ne projectiles with Mo atoms of a $2H$ -MoS₂(0001) surface as a function of the projectile incoming energy for two geometrical configurations ($\alpha/\beta = 45^\circ/90^\circ$ and $\alpha/\beta = 90^\circ/45^\circ$) while keeping the same scattering angle ($\theta_{\text{sc}} = 135^\circ$). In Fig. 3(b) we show the measured neutral fractions for two structurally different crystallographic directions, $\varphi = 0^\circ$ and $\varphi = 30^\circ$, as assessed by LEED [see inset in Fig. 1(a)] for the $\alpha/\beta = 45^\circ/90^\circ$ geometric configuration. Even when the crystalline structure of

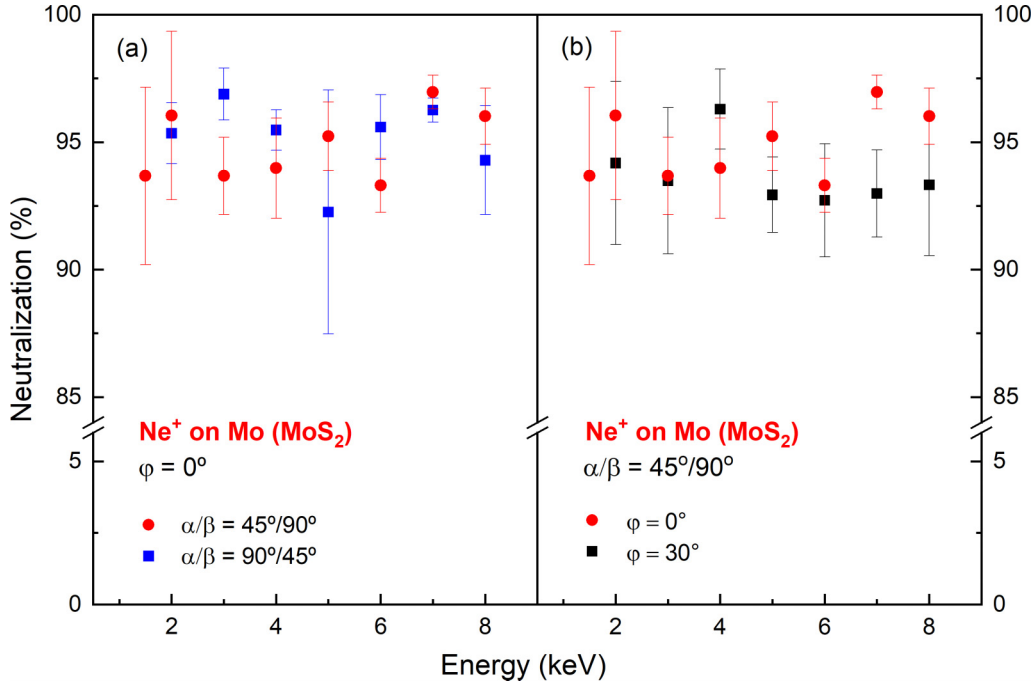


FIG. 3. Comparison of the final backscattered neutral fractions obtained after Ne^+ projectiles singly colliding with Mo atoms of an MoS_2 surface for two combinations of incoming/exit angles for $\varphi = 0^\circ$ azimuthal direction [left panel, (a)] and two different azimuthal directions, $\varphi = 0^\circ$ and $\varphi = 30^\circ$ for the $45^\circ/90^\circ$ entrance/exit angle configuration [right panel, (b)]. Almost fully neutralized backscattered projectiles are obtained independently of the incident energy, the geometrical configuration, and the crystallographic direction explored.

the $2H\text{-MoS}_2(0001)$ surface presents a threefold (120°) rotation symmetry and given the entrance/exit angles used, other relevant directions such as $\varphi = 60^\circ$ or $\varphi = 90^\circ$ are expected to be equivalent to the measured ones.

A neutralization higher than 90% is obtained for all the explored parameters: incoming energy, incoming/exit angles and crystallographic azimuthal directions. These results are consistent with the typical final charge state obtained for inert gases colliding with different surfaces [7,8,18,31,35,36,69–71]. The remaining ions (lower than 10% of the incoming projectiles) were measured to be almost totally positive [see inset of Fig. 2(b)].

The lack of dependence of the neutral fractions obtained with the different experimental parameters explored strongly suggests that the leading charge transfer mechanism is primarily ruled by the colliding atoms (Ne-Mo), with a low influence of the neighboring atoms or the surface in general. In order to experimentally explore this idea, we measured the neutral fraction obtained after Ne^+ projectiles are backscattered on a molybdenum metallic polycrystalline sample. Figure 4 shows a comparison between both the neutralization rates obtained for both samples for an incoming/exit angle of $45^\circ/90^\circ$. An average of the neutral fractions obtained for both azimuthal directions was used for the Ne-Mo (MoS_2) system.

The comparison between the experimental neutral fractions obtained for both surfaces can be summarized in five features: (i) in a general view, the neutral fractions obtained for both surfaces are quite alike in magnitude and dependence with projectile incoming energy; (ii) an efficient neutralization is taking place in both systems: neutral fractions higher than 85% are measured in the whole analyzed energy range; (iii) no appreciable differences are obtained for the neutral fractions at

energies lower than 4 keV; (iv) slightly lower neutral fractions are obtained for the polycrystalline Mo surface for energies larger than 4 keV; and (v) as a consequence of (iii) and (iv) a higher dependence with the incoming energy is obtained for the metallic surface. The similar neutral fractions obtained for these two surfaces with such different electronic properties suggest that the projectile features, such as the position of its ground state level, are more important than the details of the electronic structure of the surface.

B. Theoretical results: Resonant charge transfer contribution

In Fig. 5 we show the dependence of the Ne- $2p_z$ ionization level (E_a) with the projectile-surface distance, when a Ne projectile is directly scattered by a Mo atom of the analyzed surfaces. The local density of states of both studied surfaces are also shown. The energy positions of the core states of Mo atoms included in the calculation (Mo- $4p$ and Mo- $4s$) relative to the active electronic energy level of the projectile indicate that they play a relevant role in resonant charge transfer. These states are considered zero-width electronic energy levels. The S- $2p$ core state, positioned at -158.5 eV, was found to have no relevance in the calculation since it is not reached by the level demotion at 1 a.u. However, this state could be relevant at shorter projectile-surface distances of closest approach.

For Ne^+ colliding with the Mo atoms of the MoS_2 surface and for large projectile-surface distances ($2 \text{ a.u.} < z < 6 \text{ a.u.}$) the ionization level (Ne- $2p_z$) resonates with the bottom region of the MoS_2 valence band and then, the whole charge transfer process should be governed by the resonant mechanism in this region [4,7]. For lower ion-surface distances ($z < 2 \text{ a.u.}$), a

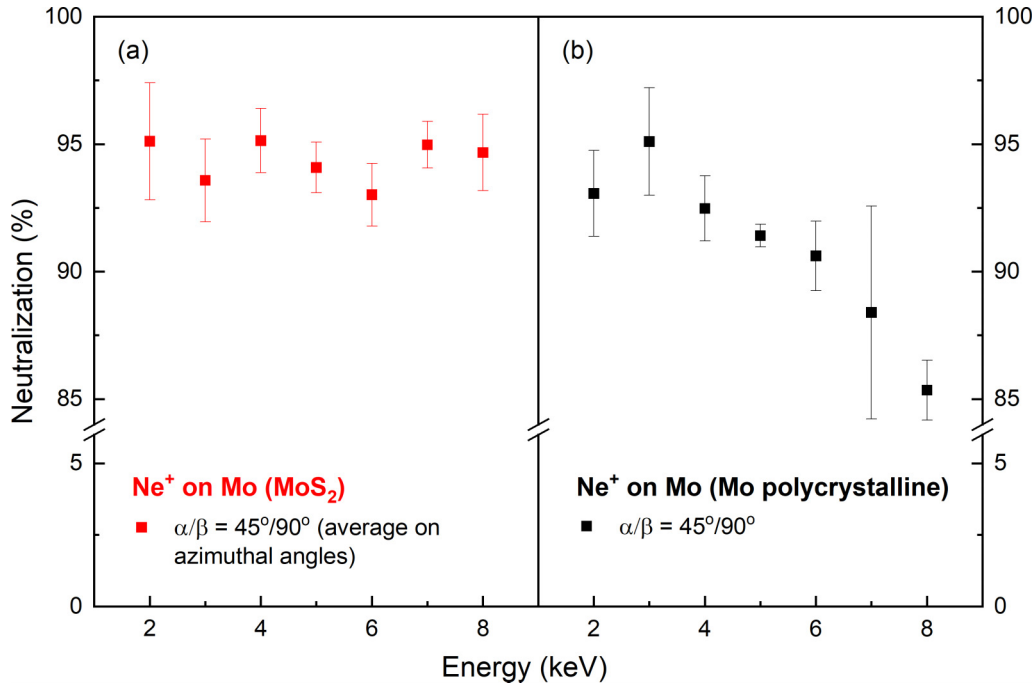


FIG. 4. Neutralization rates obtained for binary collisions of Ne⁺ projectiles backscattered by Mo atoms of a semiconducting MoS₂ surface [left panel, (a)] and a metallic polycrystalline surface [right panel, (b)].

region where the ion-surface charge exchange is still active [7,9], the ionization level lies below the bottom of the surface valence band and then, contributions other than valence-band resonant processes should become important. Then, resonant

and other charge transfer mechanisms are expected to contribute to the ion neutralization in this system.

The ionization level of Ne on the polycrystalline Mo metallic surface consistently resides well below the low-energy limit of the valence band throughout the region where charge transfer is possible (1 a.u. < z < 8 a.u.), rendering the resonant charge transfer mechanism unlikely. Therefore, and given the metallic character of the surface studied, it is expected that charge transfer via Auger mechanisms will be dominant.

In Fig. 6 we show the calculated neutral fractions due to resonant processes, contrasted to the experimental values. In this figure we can observe that, for Ne scattered by Mo in MoS₂, the contribution from the resonant mechanisms strongly decreases for increasing projectile velocities, clearly indicating that this process is more efficient for higher projectile-surface interaction times. Moreover, it explains the almost full neutralization observed at the lowest projectile incoming energy (2 keV) but only accounts for approximately half of the measured neutral fractions at higher projectile velocities. In addition, the pronounced dependence with the projectile velocity is not consistent with the nearly negligible dependence observed in the experiment. Therefore, even when the resonant mechanism primarily contributes to the projectile neutralization, it is expected that other charge transfer mechanisms will also play a significant role, especially at higher projectile velocities. On the other hand, and mostly due to the deep position of the relevant energy level, the resonant contribution only explains a minor portion of the neutralization obtained for the Mo polycrystalline surface.

Figure 7 shows the evolution of the calculated neutralization rates due to resonant processes as the Ne projectile approaches and leaves the target surface. The results are shown for the two studied surfaces for 8-keV Ne incoming projectiles. In order to show the relevance of the inner (core)

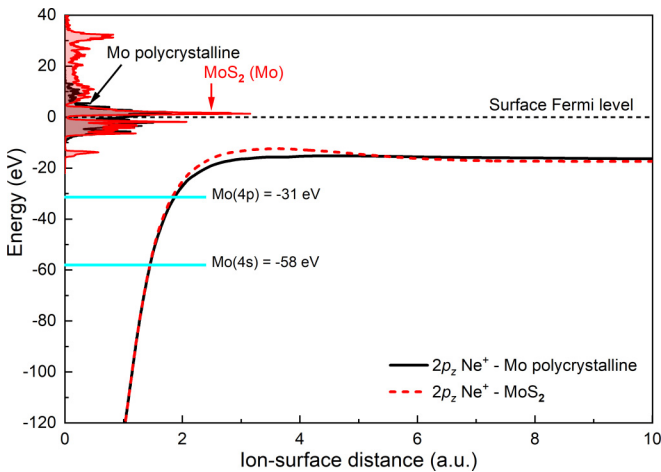


FIG. 5. Ionization energy level (Ne- $2p_z$) for the Ne projectile interacting with a Mo atom of a MoS₂ surface (red dashed line) and a Mo polycrystalline (black solid line) target as a function of the projectile-surface distance. The shadowed areas correspond to the local density of states of MoS₂ (red) and Mo polycrystalline (black) projected on the Mo atom. The energies refer to the surface Fermi level (dashed black line), where a work function of 4.54 eV was used for the MoS₂ surface [72] and 4.5 eV for metallic Mo [73]. Relevant core levels are indicated (cyan solid). The deep energy position of the active projectile energy level relative to the surface valence band suggests, at first glance, a non-negligible contribution of charge transfer mechanisms other than resonant.

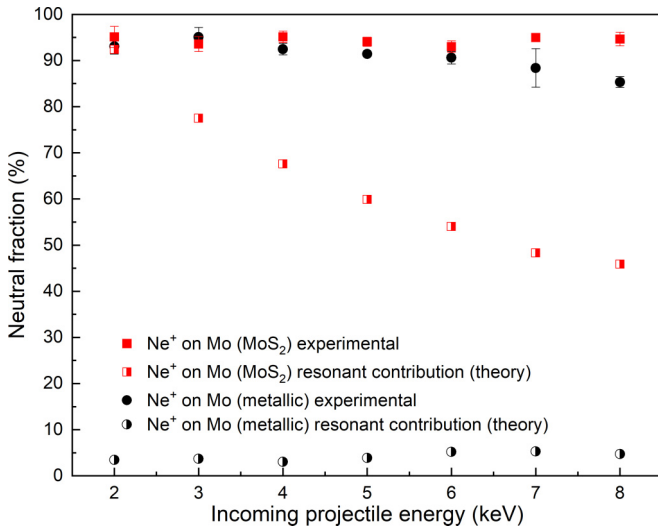


FIG. 6. Ne^+ neutralization probability as a function of the incident projectile energy for Ne directly colliding with Mo atoms. Experimental data (solid symbols) are contrasted to theoretical calculations (semiempty symbols) for the two target surfaces analyzed: molybdenum disulfide (red squares) and metallic polycrystalline molybdenum (black circles).

states in the resonant charge transfer, the neutral fraction evolutions are shown for two different situations: (i) when the core states are included in the calculation and (ii) when they are disregarded. The results for Ne projectiles colliding with MoS_2 are also presented for 2-keV incoming projectiles to explore the large variations in neutral fractions shown in Fig. 6 at the two ends of the examined incoming energy range.

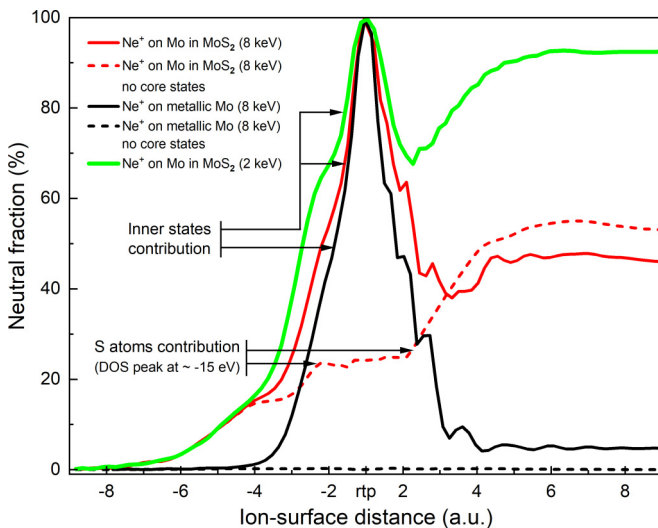


FIG. 7. Normal distance dependence of the neutral fraction due to resonant mechanisms for Ne^+ projectiles directly colliding with a Mo present in the two target surfaces studied: molybdenum disulfide and metallic molybdenum. Negative and positive values for the ion-surface distance represent incoming and exit projectile trajectories, respectively. The return point, located at 1 a.u. from the Mo atom, is indicated as “rtp.” The contrast between curves obtained when inner states are included and not included, allows us to separate contributions from the core and band states.

The analysis of the Ne on Mo (MoS_2) neutral fraction evolution indicates that resonant charge transfer mechanisms are active for ion-surface distances lower than around 8 a.u. The projectiles are fully neutralized at the end of the entrance path and subsequently, they lose part the captured electrons in the outgoing trajectory for ion-surface distances close to the surface ($1 \text{ a.u.} < z < 3 \text{ a.u.}$). In this region, there is an apparent competence between losing electrons to the inner states and capturing them from the valence band. Finally, projectiles mostly capture electrons again at the end of the outgoing path when inner states are not available. The contrast between calculations when core levels are included and not included provides crucial information to understand the process. The comparison between both plots (solid and dashed red lines) clearly indicates that the abrupt rise and fall observed in the neutralization rates for close ion-surface distances ($z < 3 \text{ a.u.}$) in the incoming and exit paths, respectively, are a direct consequence of the capture and release of electrons from and to the inner states. The oscillation observed in the neutral fractions in the outgoing path are typical of resonant processes occurring with narrow (or zero-width) density of state (DOS) peaks as exhibited by core states. On the other hand, the resonance with the valence band is active for distances larger than around 2 a.u. and contributes to electron capture as evidenced by the nearly monotonously increasing neutral fraction in the absence of inner states (red dashed line). In addition, the MoS_2 DOS peak centered at around -15 eV (see Fig. 5), is responsible for the main rises (around 2 a.u. from the surface) of the neutralization observed in Fig. 7. This DOS peak originates in the $3s$ states of the S atoms of the MoS_2 surface. The contrast between curves obtained for 2- and 8-keV incoming energies highlights the relevance of the projectile-surface interaction times in the resonant charge exchange mechanism, where the explored energy range noticeably matches the timescale of the resonant processes for this system. Shorter interaction times, associated to lower incoming energies, result in a much more efficient capture of electrons from the valence band by the projectile.

The analysis of the neutralization evolution of Ne projectiles impinging on polycrystalline Mo contains less ingredients than that of MoS_2 . Given the deep energy position of the Ne ionization level relative to the bottom of the Mo metallic valence band, the ion-surface charge exchange takes place in a more limited region ($z < 4 \text{ a.u.}$) and the ionization level can only resonate with the inner states of the Mo metallic surface. As a consequence, the valence and conduction bands do not play any significant role in the resonant charge transfer mechanism, as revealed by a fully null neutralization observed during the whole collision process when the inner core states are not considered in the calculation (black dashed line).

C. Theoretical results: Other charge transfer contributions

The substantial differences observed between the experimental data and the theoretical resonant charge exchange contributions clearly indicate that, for both samples, other charge transfer mechanisms should be included to adequately describe the measured final charge state of the Ne projectiles. On the other hand, previous studies of charge exchange when inert gases are used as projectiles indicate that Auger and

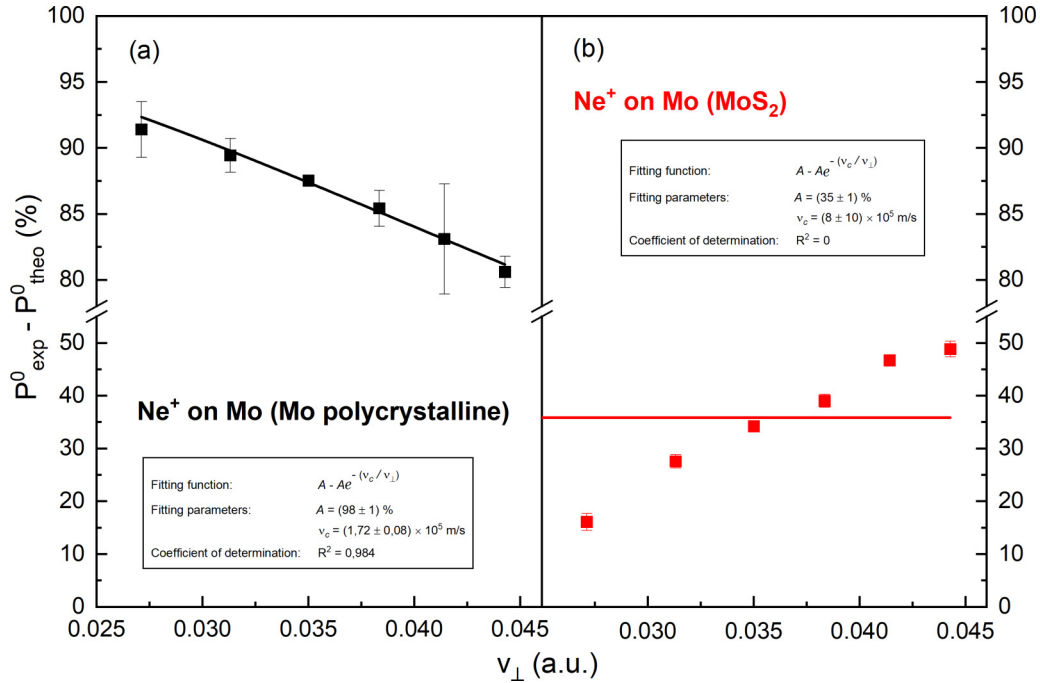


FIG. 8. Difference between the measured neutral fractions and the calculated neutralization purely due to resonant mechanisms as a function of the perpendicular velocity, v_{\perp} , for Ne projectiles colliding with Mo atoms of metallic polycrystalline molybdenum (a) and a MoS₂ surface (b). The fitting function used [Eq. (10)] and the fitting parameters obtained are indicated in the figure. The best-fit curves obtained for both systems are plotted with solid lines. Parameter A represents the weight of Auger neutralization in the total measured neutral fraction. Only a good description of the data was found for the Mo metallic sample. The poor curve fitting and parameters obtained for Ne/MoS₂ suggests that neutralization mechanisms other than resonant and Auger processes are crucial for explaining neutralization in this system.

further mechanisms other than resonant to the ionization level are dominant in these systems. For example, for noble gases colliding with metals, it has been shown that Auger neutralization mechanisms adequately explain the measured final neutral fractions [18,21,34,74], except when autoionization processes are present [17]. However, for He colliding with nonmetal surfaces such as HOPG (highly oriented pyrolytic graphite), more complex phenomena such as neutralization to the projectile ground state mediated by the correlation with He excited states through their interaction with the surface band states were shown to be relevant for a proper description of the experimental results obtained [36,56]. An Auger deexcitation process follows the resonant electron capture to the He excited states and substantially contributes to the neutralization of the ground state of the He projectiles.

Figure 8 exhibits the difference between measured and calculated neutral fractions, when only the resonant mechanism to the Ne ground state is considered, for both investigated samples. In order to examine whether only the Auger neutralization processes are responsible for the large differences observed, these data are fitted with a typical Auger neutralization probability contribution following the simple Hagstrum model [75]:

$$P_{\text{Auger}}^0 = 1 - \exp\left[\frac{-v_c}{v_{\perp}}\right], \quad (10)$$

where P_{Auger}^0 is the neutralization probability due to Auger processes, v_c is the Auger characteristic velocity for the particular system analyzed, and $v_{\perp} \equiv (v_{\text{in},\perp}^{-1} + v_{\text{out},\perp}^{-1})^{-1}$ corresponds to the general perpendicular velocity, being $v_{\text{in},\perp}$ and $v_{\text{out},\perp}$ per-

pendicular to the surface components of the incoming and outgoing projectile velocities, respectively.

The good agreement obtained between the data and the fitting function shown in Fig. 8(a) allows us to assert that neutralization for this system is mainly ruled by Auger mechanisms. Additionally, the characteristic Auger velocity obtained, $v_c = (1.72 \pm 0.08) \times 10^5 \text{ ms}^{-1}$, is quite similar to those obtained for the neutralization of Ne colliding with other transition metals such as tungsten [$v_c = (1.70 \pm 0.08) \times 10^5 \text{ ms}^{-1}$ was reported for Ne on W in [22]] and comparable to that of Ne⁺ scattered by Ba, Cu, or Au [21,22].

The visible and complete disagreement between the data points and the fitting curve shown in Fig. 8(b) for Ne colliding with MoS₂ leads us to conclude that other neutralization mechanisms, different than resonant and Auger, significantly contribute to the neutralization of Ne projectiles. The results obtained in the present system (Ne on MoS₂) resemble that obtained for the He on HOPG in [36] in many features: (i) an almost complete neutralization experimentally obtained; (ii) a very deep projectile ionization level that, at large projectile-surface distances, resonates with the bottom part of the surface valence band and at short distances resonant mechanisms are not feasible; (iii) surfaces with rather similar work functions (~ 4.5 eV) and with certain similarities in their electronic DOS (low DOS at the Fermi level, valence- and conduction-band extensions, etc.); (iv) first excited states lying very close to the surface Fermi level; and (v) neutralization values on the order of 50% are calculated due to resonant mechanisms to the ground state using the spinless approximation, with the neutral fraction mostly decreasing with

increasing projectiles' energies. Concerning the last point, a significant difference emerges in the calculated resonant neutralization for both systems at low incoming energies. These variations probably originate in the different incoming velocities, due to rather different projectile masses, resulting in larger resonant neutral fractions for Ne projectiles at low incoming energies.

In Ref. [36], the difference between the measured neutral fractions and the calculated resonant neutralization to the ground state is explained through supplementary contributions stemming from excited states of helium. These contributions, which exhibit an increasing behavior with the projectile's energy as needed in the present case, significantly enhance the neutralization process to the ground state, primarily facilitated by a strong electronic correlation between the ground and excited states of helium, via the surface valence band. Due to the above-mentioned analogies between the two systems, it seems plausible to anticipate the presence of analogous additional neutralization channels playing a crucial role in the Ne/MoS₂ system. Consequently, the lowest excited configurations of neon [Ne($2p^5 3s^1$) and Ne($2p^5 3p^1$)] are expected to serve as transient resonant channels that, followed by a subsequent Auger deexcitation process to the ground state, substantially contribute to the electronic population of the Ne ground state. However, the incorporation of this element into our model necessitates the consideration of electronic correlation among the three configurations [Ne($2p^6$), Ne($2p^5 3s^1$), and Ne($2p^5 3p^1$)], which extends beyond the scope of the present study.

On the other hand, The Fano-Lichten model [76] describes the shift and mixing of electronic levels during atomic and molecular collisions, considering how these levels are affected as interatomic distances decrease. While primarily used for atom-atom collisions, its principles can be extended to ion-solid collisions with some modifications to account for the different interaction dynamics and complex environment of a solid surface [77]. In our model, we calculate the interactions of the projectile with all relevant surface atoms at each point of its trajectory, focusing only on the promotion and demotion of the projectile's electronic levels. We assume that the electronic level shifts of the solid target are negligible compared to those of the projectile. While this assumption is correct for most of the projectile's trajectory, at very close ion-surface distances ($z < 1$ a.u.), the shifting of the target's discrete core levels could be significant. This could lead to additional neutralization through level crossing or "quasiresonances" at this range of short distances, excluded by our current calculations but accessible by the projectile.

V. CONCLUSIONS

We present here systematic measurements of the neutral fractions of Ne⁺ projectiles backscattered by Mo atoms belonging to molybdenum disulfide and metallic molybdenum polycrystalline surfaces, for projectile incoming energies in the low-energy range (2–8 keV). In order to check for the sensitivity to matrix or surface effects, the measurements were performed for two pairs of incoming/exit angles (with the same scattering angle) and a couple of azimuthal angles corresponding to nonanalogous crystallographic directions. For the MoS₂ surface, neutral fractions between 90% and 95%

were measured independently of the incoming energy, incoming/exit angles, and crystallographic directions, indicating that the physical ingredients that rule charge exchange in this system are not sufficiently varied when the projectile energy, the incoming/exit angles, and the crystallographic directions are modified. As expected, the remaining 5%–10% of scattered projectiles were measured to be mostly positive. For the molybdenum polycrystalline sample, the neutral fraction decreases with the incoming energy, showing values slightly lower than that observed in MoS₂.

We employed a quantum-mechanical formalism based on first principles to determine the neutralization probability resulting from resonant charge exchange between the Ne ionization level and the bands and inner states of both surfaces under study. After analyzing the projectile charge state evolution during the collision, we were able to arrive at the following conclusions: (i) the projectile charge state is primarily defined at the exit trajectory for both surfaces; (ii) charge exchange processes are active for ion-surface distances closer than or on the order of 8 and 4 a.u. for MoS₂ and metallic Mo, respectively; (iii) core states play a crucial role in facilitating rapid neutralization/ionization in the incoming/exit trajectories; and (iv) larger projectile-surface interaction times can be directly associated to a more efficient projectile electron capture from the valence band of the MoS₂ surface.

Theoretically, we determined that, depending on the incoming energy of the projectile, resonant neutralization to the ionization level contributes to around 50%–95% and 3%–5% of the total experimentally obtained neutral fraction for MoS₂ and metallic Mo, respectively. The remaining difference is well explained by Auger neutralization to the ground state for the Mo polycrystalline sample where a plausible Auger characteristic velocity was determined by curve fitting using a simple and well-known model. However, by following the same line of reasoning, we have concluded that other charge exchange mechanisms are necessary to account for this difference in the MoS₂ target surface.

Drawing parallels with a similar previous studied system (He⁺ on HOPG) enables us to infer that resonant neutralization from the MoS₂ surface valence band to the projectile excited states, followed by Auger deexcitation to the Ne ground state is likely to significantly contribute to the large final neutral fraction experimentally observed. An additional neutralization channel could become significant at very close projectile-surface distances due to the onset of quasiresonances resulting from the shifting of the target atoms' core levels.

ACKNOWLEDGMENTS

This work was supported by CONICET through Grant No. PIP-2021–101517, ANPCyT through Grant No. PICT-2019–03943, Universidad Nacional del Litoral (U.N.L.) through CAI+D Grant No. 50620190100034LI, and ASaCTei through Grant No. PEICID-2022–072. C.G. acknowledges to the Spanish Supercomputing Network (RES) for the computational resources provided at Altamira (IFCA) through the Projects: FI-2024-2-0032 and the Financial support by the Spanish Ministry of Research, Innovation and Universities, Project: PID2021-123112OB-C21. We also kindly acknowledge Edith C. Goldberg for helpful discussions.

- [1] D. Geng and H. Y. Yang, Recent advances in growth of novel 2D materials: Beyond graphene and transition metal dichalcogenides, *Adv. Mater.* **30**, 1800865 (2018).
- [2] K. B. M. Ismail, M. Arun Kumar, S. Mahalingam, J. Kim, and R. Atchudan, Recent advances in molybdenum disulfide and its nanocomposites for energy applications: Challenges and development, *Materials* **16**, 4471 (2023).
- [3] S. Chen, Y. Mao, G. Wang, H. Zhang, Y. Zhang, X. Chen, R. Gu, M. Zhao, and J. Wang, Molybdenum disulfide field-effect transistors with enhanced charge-injection by inserting ultrathin pentacene layer under source/drain electrodes, *Vacuum* **206**, 111500 (2022).
- [4] J. Los and J. J. C. Geerlings, Charge exchange in atom-surface collisions, *Phys. Rep.* **190**, 133 (1990).
- [5] E. C. Goldberg and F. Flores, Charge exchange in many-body time-dependent processes, *Phys. Rev. B* **45**, 8657 (1992).
- [6] H. Winter, Image charge effects in ion surface scattering, *J. Phys.: Condens. Matter* **8**, 10149 (1996).
- [7] I. K. Gainullin, Resonant charge transfer during ion scattering on metallic surfaces, *Phys. Usp.* **63**, 888 (2020).
- [8] H. H. Brongersma, M. Draxler, M. de Ridder, and P. Bauer, Surface composition analysis by low-energy ion scattering, *Surf. Sci. Rep.* **62**, 63 (2007).
- [9] V. Quintero Riascos, M. Tacca, R. Vidal, C. Gonzalez, E. C. Goldberg, and F. Bonetto, Electron capture and loss in the scattering of low-energy protons with a C_{60} monolayer deposited on Cu(111), *Phys. Rev. A* **103**, 062805 (2021).
- [10] R. A. Wilhelm, The charge exchange of slow highly charged ions at surfaces unraveled with freestanding 2D materials, *Surf. Sci. Rep.* **77**, 100577 (2022).
- [11] S. B. Luitjens, A. J. Algra, E. P. T. M. Suurmeijer, and A. L. Boers, The measurement of energy spectra of neutral particles in low energy ion scattering, *Appl. Phys.* **21**, 205 (1980).
- [12] D. P. Woodruff, Neutralisation effects in low energy ion scattering, *Nucl. Instrum. Methods Phys. Res.* **194**, 639 (1982).
- [13] P. Bauer, in *Surface and Thin Film Analysis: A Compendium of Principles, Instrumentation, and Applications*, edited by G. Friedbacher and H. Bubern (Wiley, New York, 2011).
- [14] C. V. Cushman, P. Bruner, J. Zakel, G. H. Major, B. M. Lunt, N. J. Smith, T. Grehl, and M. R. Linfoord, Low energy ion scattering (LEIS). A practical introduction to its theory, instrumentation, and applications, *Anal. Methods* **8**, 3419 (2016).
- [15] S. Průša, M. R. Linfoord, E. Vaníčková, P. Bábík, J. W. Pinder, T. Šíkola, and H. H. Brongersma, A practical guide to interpreting low energy ion scattering (LEIS) spectra, *Appl. Surf. Sci.* **657**, 158793 (2023).
- [16] F. Wyputta, R. Zimny, and H. Winter, H^- formation in grazing collisions of fast protons with an Al(111) surface, *Nucl. Instrum. Methods Phys. Res., Sect. B* **58**, 379 (1991).
- [17] T. M. Buck, W. E. Wallace, R. A. Baragiola, G. H. Wheatley, J. B. Rothman, R. J. Gorte, and J. G. Tittensor, Differences in the neutralization of 2.4–10 keV Ne^+ scattered from the Cu and Au atoms of an alloy surface, *Phys. Rev. B* **48**, 774 (1993).
- [18] R. Souda, K. Yamamoto, W. Hayami, T. Aizawa, and Y. Ishizawa, Low-energy H^+ , He^+ , N^+ , O^+ , and Ne^+ scattering from metal and ionic-compound surfaces: Neutralization and electronic excitation, *Phys. Rev. B* **51**, 4463 (1995).
- [19] R. Souda, K. Yamamoto, W. Hayami, B. Tilley, T. Aizawa, and Y. Ishizawa, Neutralization and negative-ion formation by impact of low-energy H^+ on ionic compound surfaces, *Surf. Sci.* **324**, L349 (1995).
- [20] J. E. Gayone, R. G. Pregliasco, E. A. Sánchez, and O. Grizzi, Atomic-structure characterization of a H:GaAs(110) surface by time-of-flight ion-scattering spectrometry, *Phys. Rev. B* **56**, 4194 (1997).
- [21] L. C. A. van den Oetelaar, H. E. van Benthem, J. H. J. M. Helweggen, P. J. A. Stapel, and H. H. Brongersma, Application of low-energy noble-gas ion scattering to the quantitative surface compositional analysis of binary alloys and metal oxides, *Surf. Interface Anal.* **26**, 537 (1998).
- [22] R. Cortenraad, A. W. D. van der Gon, H. H. Brongersma, S. N. Ermolov, and V. G. Glebovsky, Work function dependent neutralization of low-energy noble gas ions, *Phys. Rev. B* **65**, 195414 (2002).
- [23] Y. Yang and J. A. Yarmoff, Charge exchange in Li scattering from Si surfaces, *Phys. Rev. Lett.* **89**, 196102 (2002).
- [24] J. O. Lugo, E. C. Goldberg, E. A. Sánchez, and O. Grizzi, Charge exchange in 3–30 keV H^+ scattering off clean and AlF_3 covered Al(111) surfaces I. Experimental study, *Phys. Rev. B* **72**, 035432 (2005).
- [25] F. Bonetto, M. A. Romero, E. A. García, R. Vidal, J. Ferrón, and E. C. Goldberg, Relevant effects of localized atomic interactions and surface density of states on charge transfer in ion-surface collisions, *Europhys. Lett.* **80**, 53002 (2007).
- [26] F. Bonetto, M. A. Romero, E. A. García, R. A. Vidal, J. Ferrón, and E. C. Goldberg, Large neutral fractions in collisions of Li^+ with a highly oriented pyrolytic graphite surface: Resonant and Auger mechanisms, *Phys. Rev. B* **78**, 075422 (2008).
- [27] B. Bahrim, S. Yu, B. Makarenko, and J. W. Rabalais, Electron dynamics in $\text{H}^-/\text{Na}/\text{Cu}(111)$ collisions, *Surf. Sci.* **603**, 703 (2009).
- [28] S. Průša *et al.*, Highly sensitive detection of surface and intercalated impurities in graphene by LEIS, *Langmuir* **31**, 9628 (2015).
- [29] L. Chen, J. Lu, P. Liu, L. Gao, Y. Liu, F. Xiong, S. Qiu, X. Qiu, Y. Guo, and X. Chen, Dissociation and charge transfer of H_2O on Cu(110) probed in real time using ion scattering spectroscopy, *Langmuir* **32**, 12047 (2016).
- [30] L. Gao *et al.*, Dynamical resonant neutralization of low-energy N^+ ions scattered from Au(111), Pd(111), Cu(111), and Cu(110) surfaces, *Phys. Rev. A* **96**, 052705 (2017).
- [31] P. Riccardi, A. Sindona, and C. A. Dukes, Local charge exchange of He^+ ions at aluminum surfaces, *Phys. Lett. A* **381**, 1174 (2017).
- [32] M. S. Tacca, F. Bonetto, and E. C. Goldberg, Electronic correlation effects on the neutralization of Ga^+ scattered by a gold surface, *Phys. Rev. B* **96**, 075424 (2017).
- [33] M. Tacca, V. Quintero Riascos, R. Vidal, C. Gonzalez, F. Bonetto, and E. C. Goldberg, Charge transfer in low-energy collisions of protons with a thick C_{60} film, *J. Phys. Chem. C* **124**, 3632 (2020).
- [34] J. M. Sturm, H. W. Lokhorst, A. A. Zameshin, and M. D. Ackermann, Charge exchange between He^+ ions and solid targets: The dependence on target electronic structure revisited, *Nucl. Instrum. Methods Phys. Res., Sect. B* **538**, 47 (2023).
- [35] N. B. Luna, F. J. Bonetto, R. A. Vidal, E. C. Goldberg, and J. Ferrón, Low energy ion scattering in He/HOPG system, *J. Mol. Catal. A: Chem.* **281**, 237 (2008).

- [36] A. Iglesias-García, F. Bonetto, R. Vidal, J. Ferrón, and E. C. Goldberg, Ion neutralization and high-energy electron emission in He^+ scattering by a highly oriented pyrolytic graphite surface, *Phys. Rev. A* **89**, 042702 (2014).
- [37] F. Bonetto, R. A. Vidal, V. Q. Riascos, C. J. Bonin, and J. Ferrón, Growth, thermal desorption and low dose ion bombardment damage of C_{60} films deposited on Cu(111), *J. Phys. Commun.* **1**, 045004 (2017).
- [38] P. G. Bolcatto, E. C. Goldberg, and M. C. G. Passeggi, Interaction between atoms and surfaces: A bond-pair description based on an extended Anderson model, *Phys. Rev. B* **58**, 5007 (1998).
- [39] A. C. Hewson, *The Kondo Problem to Heavy Fermions*, Cambridge Studies in Magnetism (Cambridge University Press, Cambridge, 1993).
- [40] H. Winter, Collisions of atoms and ions with surfaces under grazing incidence, *Phys. Rep.* **367**, 387 (2002).
- [41] F. Bonetto, C. Gonzalez, and E. C. Goldberg, Signals of strong electronic correlation in ion scattering processes, *Phys. Rev. B* **93**, 195439 (2016).
- [42] F. J. Bonetto, M. A. Romero, A. Iglesias-García, R. A. Vidal, and E. C. Goldberg, Time–energy uncertainty and electronic correlation in H^+ –graphite collisions, *J. Phys. Chem. C* **119**, 3124 (2015).
- [43] F. J. Bonetto, E. A. García, C. González, and E. C. Goldberg, Image potential state influence on charge exchange in Li^+ –metal surface collisions, *J. Phys. Chem. C* **118**, 8359 (2014).
- [44] R. A. Vidal, F. Bonetto, J. Ferrón, M. A. Romero, E. A. García, and E. C. Goldberg, Electron capture and loss in the scattering of H^+ from HOPG graphite, *Surf. Sci.* **605**, 18 (2011).
- [45] E. A. García, M. A. Romero, C. González, and E. C. Goldberg, Neutralization of Li^+ ions scattered by the Cu (100) and (111) surfaces: A localized picture of the atom-surface interaction, *Surf. Sci.* **603**, 597 (2009).
- [46] F. Bonetto, E. A. García, R. Vidal, J. Ferrón, and E. C. Goldberg, Experimental and theoretical study of charge transfer in hydrogen ion scattering from a graphite surface, *Appl. Surf. Sci.* **254**, 62 (2007).
- [47] J. O. Lugo, E. C. Goldberg, E. A. Sánchez, and O. Grizzi, Charge exchange in H^+ grazing scattering off clean and AlF_3 covered Al(111) surfaces, *Phys. Status Solidi A* **201**, 2356 (2004).
- [48] O. Grizzi, M. Shi, H. Bu, and J. W. Rabalais, Time-of-flight scattering and recoiling spectrometer (TOF-SARS) for surface analysis, *Rev. Sci. Instrum.* **61**, 740 (1990).
- [49] S. Mattila, J. A. Leiro, M. Heinonen, and T. Laiho, Core level spectroscopy of MoS_2 , *Surf. Sci.* **600**, 5168 (2006).
- [50] Z. Dai, W. Jin, M. Grady, J. T. Sadowski, J. I. Dadap, R. M. Osgood, and K. Pohl, Surface structure of bulk $2\text{H-MoS}_2(0001)$ and exfoliated suspended monolayer MoS_2 : A selected area low energy electron diffraction study, *Surf. Sci.* **660**, 16 (2017).
- [51] C. Meyer, F. Bonetto, R. Vidal, E. A. García, C. Gonzalez, J. Ferrón, and E. C. Goldberg, Understanding the high neutralization yields in collisions of keV Li^+ ions with copper surfaces, *Phys. Rev. A* **86**, 032901 (2012).
- [52] V. Q. Riascos, M. Tacca, R. Vidal, C. Gonzalez, E. C. Goldberg, and F. Bonetto, Band structure effects on the charge exchange processes in H^+ colliding with a Cu(111) surface, *J. Phys. Chem. C* **122**, 28192 (2018).
- [53] P. W. Anderson, Localized magnetic states in metals, *Phys. Rev.* **124**, 41 (1961).
- [54] D. Primetzhofer, M. Spitz, E. Taglauer, and P. Bauer, Resonant charge transfer in low-energy ion scattering: Information depth in the reionization regime, *Surf. Sci.* **605**, 1913 (2011).
- [55] E. A. García, P. G. Bolcatto, M. C. G. Passeggi, and E. C. Goldberg, Hydrogen scattering from a LiF ionic surface: Madelung potential and local environment effects, *Phys. Rev. B* **59**, 13370 (1999).
- [56] A. Iglesias-García, E. A. García, and E. C. Goldberg, Role of He excited configurations in the neutralization of He^+ ions colliding with a HOPG surface, *Phys. Rev. B* **87**, 075434 (2013).
- [57] M. A. Romero, A. Iglesias-García, E. A. García, and E. C. Goldberg, Hydrogen ion scattering from a potassium impurity adsorbed on graphene, *Phys. Rev. B* **100**, 085432 (2019).
- [58] A. Iglesias-García, C. González, and E. C. Goldberg, Theoretical study of the charge transfer and electron emission in the scattering of He^+ by an AlF_3 surface, *Phys. Rev. B* **96**, 075428 (2017).
- [59] S. Huzinaga, Gaussian-type functions for polyatomic systems. I, *J. Chem. Phys.* **42**, 1293 (1965).
- [60] S. Huzinaga, J. Andzelm, M. Klobukowsky, E. Radzio-Andzelm, Y. Sakai, and H. Tatewaki, *Gaussian Basis Sets for Molecular Calculations* (Elsevier, Amsterdam, 1984).
- [61] J. F. Ziegler and J. P. Biersack, in *Treatise on Heavy-Ion Science, Volume 6: Astrophysics, Chemistry, and Condensed Matter*, edited by D. A. Bromley (Springer US, Boston, MA, 1985), pp. 93.
- [62] L. V. Keldysh, Diagram technique for nonequilibrium processes, *Sov. Phys. JETP* **20**, 1018 (1965).
- [63] J. P. Lewis *et al.*, Advances and applications in the FIREBALL *ab initio* tight-binding molecular-dynamics formalism, *Phys. Status Solidi B* **248**, 1989 (2011).
- [64] P. Jelínek, H. Wang, J. P. Lewis, O. F. Sankey, and J. Ortega, Multicenter approach to the exchange-correlation interactions in *ab initio* tight-binding methods, *Phys. Rev. B* **71**, 235101 (2005).
- [65] N. Troullier and J. L. Martins, Efficient pseudopotentials for plane-wave calculations, *Phys. Rev. B* **43**, 1993 (1991).
- [66] C. González and Y. J. Dappe, Molecular detection on a defective MoS_2 monolayer by simultaneous conductance and force simulations, *Phys. Rev. B* **95**, 214105 (2017).
- [67] N. Wakabayashi, H. G. Smith, and R. M. Nicklow, Lattice dynamics of hexagonal MoS_2 studied by neutron scattering, *Phys. Rev. B* **12**, 659 (1975).
- [68] M. Romero, A. Iglesias-García, and E. C. Goldberg, Quantum-mechanical interference in charge exchange between hydrogen and graphene-like surfaces, *J. Phys.: Condens. Matter* **24**, 045004 (2012).
- [69] H. H. Brongersma and T. M. Buck, Selected topics in low-energy ion scattering: Surface segregation in Cu/Ni alloys and ion neutralization, *Surf. Sci.* **53**, 649 (1975).
- [70] R. Souda, M. Aono, C. Oshima, S. Otani, and Y. Ishizawa, Mechanism of electron exchange between low energy He^+ and solid surfaces, *Surf. Sci. Lett.* **150**, L59 (1985).

- [71] J. A. Yarmoff and R. S. Williams, Neutralization effects in impact collision ion scattering spectroscopy: ⁶Li⁺ versus ⁴He⁺, *Surf. Sci.* **166**, 101 (1986).
- [72] S. Y. Lee *et al.*, Large work function modulation of monolayer MoS₂ by ambient gases, *ACS Nano* **10**, 6100 (2016).
- [73] J. Hölzl and F. K. Schulte, in *Solid Surface Physics*, edited by J. Hölzl, F. K. Schulte, and H. Wagner (Springer, Berlin, Heidelberg, 1979), p. 1.
- [74] M. Draxler, J. E. Valdés, R. Beikler, and P. Bauer, On the extraction of neutralisation information from low energy ion scattering spectra, *Nucl. Instrum. Methods Phys. Res., Sect. B* **230**, 290 (2005).
- [75] H. D. Hagstrum, Theory of Auger ejection of electrons from metals by ions, *Phys. Rev.* **96**, 336 (1954).
- [76] U. Fano and W. Lichten, Interpretation of Ar⁺-Ar collisions at 50 KeV, *Phys. Rev. Lett.* **14**, 627 (1965).
- [77] P. Riccardi and C. A. Dukes, Effects of the solid target on electronic excitations during binary atomic collisions in the interaction of Ne ions with Al surfaces, *Vacuum* **204**, 111393 (2022).